Title
Propagation of p-polarized surface plasmon polaritons circumferentially around a locally cylindrical surface

Journal
Optics Communications, 316

ISSN
0030-4018

Authors
Polanco, J
Fitzgerald, RM
Maradudin, AA

Publication Date
2014-04-01

DOI
10.1016/j.optcom.2013.12.003

Optics Communications 316 (2014) 120–126

Contents lists available at ScienceDirect

Optics Communications

journal homepage: www.elsevier.com/locate/optcom

Propagation of p-polarized surface plasmon polaritons circumferentially around a locally cylindrical surface

J. Polanco [a], R.M. Fitzgerald [b,*], A.A. Maradudin [c]

[a] Program in Computer Science, University of Texas, El Paso, TX 79968, USA
[b] Department of Physics, University of Texas, El Paso, 500 W. University Avenue, El Paso, TX 79968, USA
[c] Department of Physics and Astronomy, University of California, Irvine, CA 92697, USA

ARTICLE INFO

Article history:
Received 20 September 2013
Received in revised form
21 November 2013
Accepted 1 December 2013
Available online 12 December 2013

Keywords:
Guided plasmon polaritons
Cylindrical boundary
Circumferential propagation

ABSTRACT

We study properties of a p-polarized surface plasmon polariton propagating circumferentially around a portion of a cylindrical interface between a vacuum and a metal, a situation investigated earlier by Berry (J. Phys. A: Math. Gen. 8 (1975) 1952). When the metal is convex toward the vacuum this mode is radiative and consequently is attenuated as it propagates on the cylindrical surface. An approximate analytic solution of the dispersion relation for this wave is obtained by an approach different from the one used by Berry, and plots of the real and imaginary parts of its wave number are presented. When the metal is concave to the vacuum, the resulting dispersion relation possesses a multiplicity of solutions that have the nature of waveguide modes that owe their existence to the curvature of the interface.

1. Introduction

The propagation of a p-polarized surface electromagnetic wave circumferentially around a portion of a cylindrical boundary between a vacuum and a metal was studied by Berry [1]. Among the results obtained in this work was the result that when the metal is convex toward the vacuum the wave is not perfectly bound to the interface, but is attenuated as it propagates around it, the lost energy being radiated to infinity in the vacuum. In contrast, when the metal is concave toward the vacuum, no attenuation of the wave occurs, and the wave is a true surface wave bound to the interface.

In this paper we extend Berry's results in two directions. For the case where the metal is convex to the vacuum, we present an approximate analytic solution of the corresponding dispersion relation by a method suggested by Berry. This method of solution may be of some interest in itself. We also provide plots of the real and imaginary parts of the wavenumber provided by this solution, and compare them with the corresponding functions obtained by a purely numerical approach. In the case when the metal is concave to the vacuum, we show that the corresponding dispersion relation has a multiplicity of solutions that have the nature of guided waves confined to the vicinity of the interface by its curvature. Plots of the dispersion curves and magnetic field profiles of these waves are presented.

2. Dispersion relations and field profiles

In studying the propagation of a p-polarized surface plasmon polariton circumferentially around a portion of a cylindrical interface of radius R between a vacuum and a metal it is convenient to work in cylindrical coordinates (r,θ,z), where the z-axis is along the axis of the cylinder. The metal is characterized by an isotropic, frequency-dependent dielectric function $\varepsilon(\omega)$. For simplicity we initially assume that $\varepsilon(\omega)$ is real, and has the simple free-electron form

$$\varepsilon(\omega)=1-\frac{\omega_p^2}{\omega^2}, \tag{1}$$

where ω_p is the plasma frequency of the electrons in the metal. The only nonzero components of the magnetic and electric fields in this system are $H_z(r,\theta|\omega)$, $E_r(r,\theta|\omega)$ and $E_\theta(r,\theta|\omega)$, where

$$E_r(r,\theta|\omega)=i\frac{c}{\omega\varepsilon}\frac{1}{r}\frac{\partial H_z(r,\theta|\omega)}{\partial\theta} \tag{2a}$$

$$E_\theta(r,\theta|\omega)=-i\frac{c}{\omega\varepsilon}\frac{\partial H_z(r,\theta|\omega)}{\partial r}, \tag{2b}$$

and ε is the dielectric function of the medium in which the field is being calculated. In writing Eqs. (2) we have assumed a time dependence for the fields given by $\exp(-i\omega t)$, but have not indicated this explicitly.

The Maxwell equation satisfied by $H_z(r,\theta|\omega)$ is

$$\frac{1}{r}\frac{\partial}{\partial r}\left(r\frac{\partial H_z}{\partial r}\right)+\frac{1}{r^2}\frac{\partial^2 H_z}{\partial\theta^2}+\varepsilon(\omega)\frac{\omega^2}{c^2}H_z=0 \tag{3a}$$

* Corresponding author.
E-mail address: rfitzgerald@utep.edu (R.M. Fitzgerald).

0030-4018/$ - see front matter © 2013 Elsevier B.V. All rights reserved.
http://dx.doi.org/10.1016/j.optcom.2013.12.003

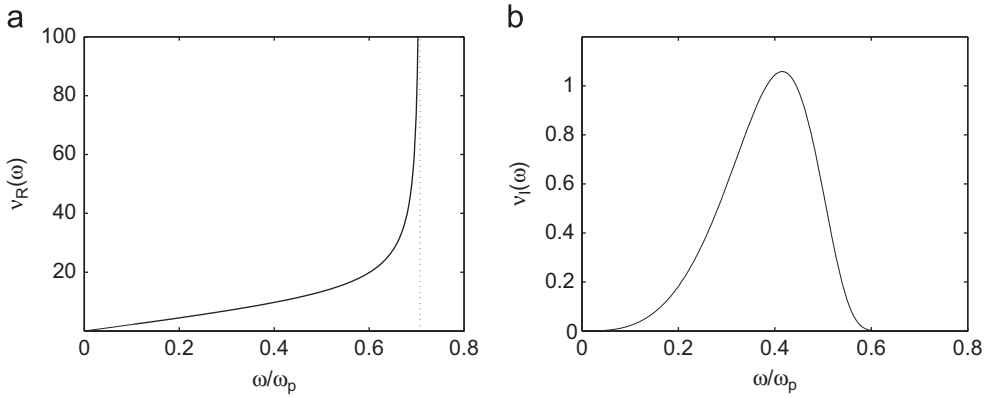

Fig. 1. Plots of $k_R(\omega)R$ (a) and the corresponding $k_I(\omega)R$ (b) as functions of the frequency ω for a leaky p-polarized surface plasmon polariton propagating circumferentially on a portion of a cylindrical silver surface that is convex to the vacuum. $R=0.5$ μm, $\omega_p=13.12\times10^{15}$ s^{-1}.

inside the metal, and

$$\frac{1}{r}\frac{\partial}{\partial r}\left(r\frac{\partial H_z}{\partial r}\right)+\frac{1}{r^2}\frac{\partial^2 H_z}{\partial\theta^2}+\frac{\omega^2}{c^2}H_z=0, \tag{3b}$$

in the vacuum in contact with it. The boundary conditions satisfied by $H_z(r,\theta|\omega)$ at the interface $r=R$ are

$$H_z(r,\theta|\omega)|_{r=R-}=H_z(r,\theta|\omega)|_{r=R+} \tag{4a}$$

$$\frac{1}{\varepsilon_-}\frac{\partial}{\partial r}H_z(r,\theta|\omega)|_{r=R-}=\frac{1}{\varepsilon_+}\frac{\partial}{\partial r}H_z(r,\theta|\omega)|_{r=R+}, \tag{4b}$$

which express the continuity of the tangential components of the magnetic and electric fields, respectively, across this interface. The quantities ε_+ and ε_- are the dielectric functions of the media in the regions $r>R$ and $r<R$, respectively.

We solve Eqs. (3a) and (3b) by separation of variables, and write

$$H_z(r,\theta|\omega)=R(r)\Theta(\theta). \tag{5}$$

We find that $R(r)$ and $\Theta(\theta)$ satisfy the following equations

$$\frac{d^2R}{dr^2}+\frac{1}{r}\frac{dR}{dr}+\left(\varepsilon\frac{\omega^2}{c^2}-\frac{\nu^2}{r^2}\right)R=0 \tag{6}$$

$$\frac{d^2\Theta}{d\theta^2}+\nu^2\Theta=0, \tag{7}$$

respectively, where ε is the dielectric function of the medium in which the field is being calculated, and ν is the separation constant. We will choose the solution of Eq. (7) to be $\exp(i\nu\theta)$, with ν real and positive. It thus describes a wave propagating circumferentially around the cylinder. The separation constant ν is not required to be an integer because we are not considering a complete cylinder, but only a locally cylindrical surface. If we write $\exp(i\nu\theta)$ as $\exp[i(\nu/R)(R\theta)]$ and recall that $R\theta=s$ measures distance along the cylindrical surface, we see that $(\nu/R)=k$ has the physical significance of a surface wave number.

There are now two cases to consider: (i) the metal is convex toward the vacuum; and (ii) the metal is concave toward the vacuum. We consider them in turn.

(i) *The metal is convex toward the vacuum*: In this case the metal occupies the region $r<R$, while the vacuum occupies the region $r>R$. Eq. (6) takes the following forms in these two regions:

$$\frac{d^2R^<}{dr^2}+\frac{1}{r}\frac{dR^<}{dr}+\left(\varepsilon(\omega)\frac{\omega^2}{c^2}-\frac{\nu^2}{r^2}\right)R^<=0,\quad 0\le r\le R \tag{8a}$$

$$\frac{d^2R^>}{dr^2}+\frac{1}{r}\frac{dR^>}{dr}+\left(\frac{\omega^2}{c^2}-\frac{\nu^2}{r^2}\right)R^>=0,\quad r\ge R. \tag{8b}$$

The solutions of these equations are Bessel functions. We seek a solution of Eq. (8a) that decays exponentially with increasing distance from the surface $r=R$ toward the origin $r=0$, as is required for a surface wave. Such a solution is possible if $\varepsilon(\omega)<0$, in which case it is given by $R^<(r)=I_\nu(|\varepsilon(\omega)|^{1/2}(\omega/c)r)$, where $I_\nu(x)$ is the modified Bessel function of the first kind and order ν. In the case of Eq. (8b) we choose for its solution $R^>(r)=H_\nu^{(1)}((\omega/c)r)$ where $H_\nu^{(1)}(x)$ is the Hankel function of the first kind and order ν. In choosing this solution we have used the fact that all solutions of Eq. (8b) are oscillatory functions of r, and the one we have chosen is the only one that describes an outgoing wave as $r\to\infty$. Thus, we find that p-polarized surface electromagnetic waves that decay with increasing r cannot exist in the situation under consideration: they must radiate. The magnetic field in our system is therefore written as

$$H_z(r,\theta|\omega)=AI_\nu(|\varepsilon(\omega)|^{1/2}(\omega/c)r)\exp(i\nu\theta),\quad 0\le r\le R \tag{9a}$$

$$=BH_\nu^{(1)}((\omega/c)r)\exp(i\nu\theta),\quad r\ge R. \tag{9b}$$

Substitution of these expressions into the boundary conditions (4) yields the solvability condition as

$$\frac{I_\nu'(|\varepsilon(\omega)|^{1/2}(\omega/c)R)}{I_\nu(|\varepsilon(\omega)|^{1/2}(\omega/c)R)}=-|\varepsilon(\omega)|^{1/2}\frac{H_\nu^{(1)'}((\omega/c)R)}{H_\nu^{(1)}((\omega/c)R)}, \tag{10}$$

where a prime denotes differentiation with respect to argument. Eq. (10) is the dispersion relation for p-polarized surface plasmon polaritons in the present case. Its solution gives $\nu=kR$ as a function of ω. However, Eq. (10) has no real solution, and the surface wave number $k(\omega)$ is a complex quantity, $k(\omega)=k_R(\omega)+ik_I(\omega)$. This result expresses the fact that the surface plasmon polariton is attenuated as it propagates around the cylinder, even in the absence of ohmic losses in the metal, because it radiates as it travels along the surface, and energy conservation requires that the energy radiated must be extracted from the wave itself.

An approximate analytic solution of Eq. (10) was obtained by Berry [1], by means of a physically based approach. It is given by

$$k_R(\omega)=\frac{\nu_R(\omega)}{R}=\frac{\omega}{c}\left[\frac{|\varepsilon(\omega)|}{|\varepsilon(\omega)|-1}\right]^{1/2} \tag{11a}$$

$$k_I(\omega)=\frac{\nu_I(\omega)}{R}=\frac{\omega}{c}\frac{|\varepsilon(\omega)|^{3/2}}{(|\varepsilon(\omega)|-1)^{3/2}(|\varepsilon(\omega)|+1)}\times\exp\left\{-\frac{(\omega/c)R}{(|\varepsilon(\omega)|-1)^{1/2}}\left[|\varepsilon(\omega)|^{1/2}\ln\frac{|\varepsilon(\omega)|^{1/2}+1}{|\varepsilon(\omega)|^{1/2}-1}-2\right]\right\}. \tag{11b}$$

A derivation of these results by an approach suggested by Berry is presented in the Appendix. In Fig. 1(a) and (b) we plot $k_R(\omega)R$

and $k_I(\omega)R$, respectively, as functions of ω/ω_p for a cylindrical silver surface. In their calculation we have used the value $\omega_p = 13.12 \times 10^{15}\ s^{-1}$. This value was obtained by fitting Eq. (1) to the real part of the dielectric constant of silver at a wavelength $\lambda = 612.7$ nm, namely $\varepsilon(\omega) = -17.2 + i0.498$ [2]. The value of the radius R assumed in these calculations was $R = 0.5$ μm. It is seen that $\nu_I(\omega)/R$ is indeed much smaller than $\nu_R(\omega)/R$, justifying the perturbative treatment used in the Appendix to obtain $\nu_I(\omega)/R$.

The approximate analytic results given by Eqs. (11a) and (11b) have been checked numerically. For a chosen value of ω Eq. (10) is rewritten as

$$f(\nu) = 0, \tag{12}$$

where

$$f(\nu) = \frac{I_\nu'(|\varepsilon(\omega)|^{1/2}(\omega/c)R)}{I_\nu(|\varepsilon(\omega)|^{1/2}(\omega/c)R)} + |\varepsilon(\omega)|^{1/2}\frac{H_\nu^{(1)'}((\omega/c)R)}{H_\nu^{(1)}((\omega/c)R)}. \tag{13}$$

We denote by ν_0 a complex estimate of the solution of Eq. (12) for a chosen value of ω. Newton's method [3] tells us that an improved approximation to the solution is

$$\nu_1 = \nu_0 - \frac{f(\nu_0)}{f'(\nu_0)}. \tag{14}$$

By iterating this approach we have that

$$\nu_{n+1} = \nu_n - \frac{f(\nu_n)}{f'(\nu_n)}, \tag{15}$$

and the solution we seek is given by $\nu = \lim_{n\to\infty}\nu_n$. A new value of ω is chosen, and the process is repeated. In this way the functions $\nu_R(\omega)$ and $\nu_I(\omega)$ are determined as functions of ω.

The ratios $H_\nu^{(1)'}((\omega/c)R)/H_\nu^{(1)}((\omega/c)R)$ and $I_\nu'(|\varepsilon(\omega)|^{1/2}(\omega/c)R)/I_\nu(|\varepsilon(\omega)|^{1/2}\times(\omega/c)R)$ were calculated as functions of ν for a chosen value of ω from continued fraction representations of them given by formulas 17.1.51 and 17.2.38 on pages 353 and 363, respectively, of Ref. [4]. The evaluation of the continued fractions was carried out by means of the modified Lenz algorithm found on page 185 of Ref. [5]. The derivative $f(\nu_n)$ entering Eq. (15) was obtained by numerical differentiation.

The results of these calculations are presented in Fig. 2(a) and (b). In Fig. 2(a) we plot $\nu_R(\omega) = k_R(\omega)R$ obtained both numerically (solid curve) and from Eq. (11a) (dashed curve). On the scale of the figure the agreement between the two results is seen to be quite good, especially for $\omega/\omega_p > 0.55$ in agreement with Berry's estimate for the domain of validity of Eq. (11a) (see the Appendix).

In Fig. 2(b) we plot the corresponding results for $\nu_I(\omega) = k_I(\omega)R$ obtained both numerically (solid curve) and from Eq. (11b) (dashed curve). We see that while the two results agree with respect to the overall magnitude of this function, and the frequency region within which this function is nonzero, they differ in shape, with the numerical result larger than the approximate result at low frequencies. This difference appears to be due to the Debye formulas used in representing the Hankel function $H^{(1)}((\omega/c)R)$ in obtaining Eqs. (11) (see the Appendix) being less accurate at low frequencies than at high frequencies.

Because the surface wave number k is given by (ν/R), the energy propagation length of the surface wave along the curved surface is given by $\ell_c(\omega) = [2k_I(\omega)]^{-1} = R/[2\nu_I(\omega)]$. The energy propagation length of a surface plasmon polariton at a planar vacuum–metal interface due to ohmic losses in the metal is given by $\ell_p(\omega) = (c/\omega)|\varepsilon_1(\omega)|^{1/2}(|\varepsilon_1(\omega)|-1)^{3/2}/\varepsilon_2(\omega)$, where $\varepsilon_1(\omega)$ and $\varepsilon_2(\omega)$ are the real and imaginary parts of the dielectric function of the metal, $\varepsilon(\omega) = \varepsilon_1(\omega) + i\varepsilon_2(\omega)$. In writing the expression for $\ell_p(\omega)$ we have taken into account explicitly that we are working in a frequency range where $\varepsilon_1(\omega)$ is negative. In Fig. 3 we plot both $\ell_c(\omega)$ (——) and $\ell_p(\omega)$ (- - - - -) as functions of the dimensionless frequency ω/ω_p. In Fig. 3(a) $\ell_c(\omega)$ is calculated on the basis of the result for $k_I(\omega)$ given by Eq. (11b), while in Fig. 3(b) $\ell_c(\omega)$ is calculated on the basis of the numerical result for $\nu_I(\omega)$ plotted in Fig. 2(b). From these results we see that in the visible region of the electromagnetic spectrum ($\lambda = 612.7$ nm corresponds to $\omega/\omega_p = 0.234$), where the radius of curvature of the surface is comparable to the wavelength of the surface wave, $\ell_c(\omega)$ is several orders of magnitude smaller than $\ell_p(\omega)$. Thus the radiative losses are significantly greater than the ohmic losses. A much larger value of R or working at higher frequencies is needed for these two propagation lengths to become comparable.

(ii) *The metal is concave toward the vacuum*: In this case the metal occupies the region $r > R$, while the vacuum occupies the region $0 < r < R$. Eq. (6) takes the following forms in these regions

$$\frac{d^2R^<}{dr^2} + \frac{1}{r}\frac{dR^<}{dr} + \left(\frac{\omega^2}{c^2} - \frac{\nu^2}{r^2}\right)R^< = 0, \quad 0 \le r \le R \tag{16a}$$

$$\frac{d^2R^>}{dr^2} + \frac{1}{r}\frac{dR^>}{dr} + \left(\varepsilon(\omega)\frac{\omega^2}{c^2} - \frac{\nu^2}{r^2}\right)R^> = 0, \quad r \ge R. \tag{16b}$$

The solutions of these equations are Bessel functions. For the solution of Eq. (16a) we choose $J_\nu((\omega/c)r)$. This choice is dictated by the following consideration. The Bessel function $J_\nu(x)$ for a fixed value of real nonzero ν increases exponentially with increasing x until a value $x = \nu$ is reached, at which it acquires an oscillatory dependence that continues for $x > \nu$. Such an oscillatory dependence of $J_\nu((\omega/c)r)$ for $r \sim R$ makes it possible to satisfy the boundary conditions at $r = R$. As we seek a solution for r in the range $0 \le r \le R$ that is localized for r in the vicinity of R, i.e. is small as $r \to 0$, $J_\nu((\omega/c)r)$ has this behavior provided that ν is of the order

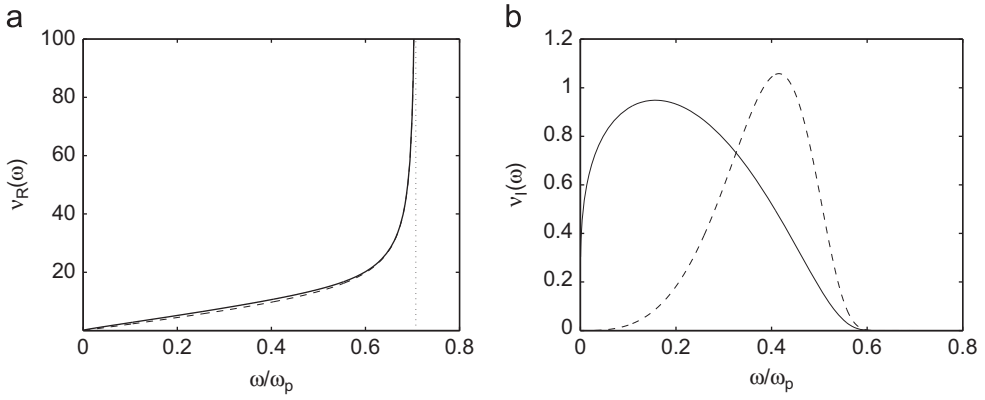

Fig. 2. Plots of $k_R(\omega)R$ (a) and the corresponding $k_I(\omega)R$ (b) as functions of the frequency ω for a leaky p-polarized surface plasmon polariton propagating circumferentially on a portion of a cylindrical silver surface that is convex to the vacuum. Numerical solution (——); approximate solution given by Eqs. (11) (- - - - -). $R = 0.5$ μm, $\omega_p = 13.12 \times 10^{15}\ s^{-1}$.

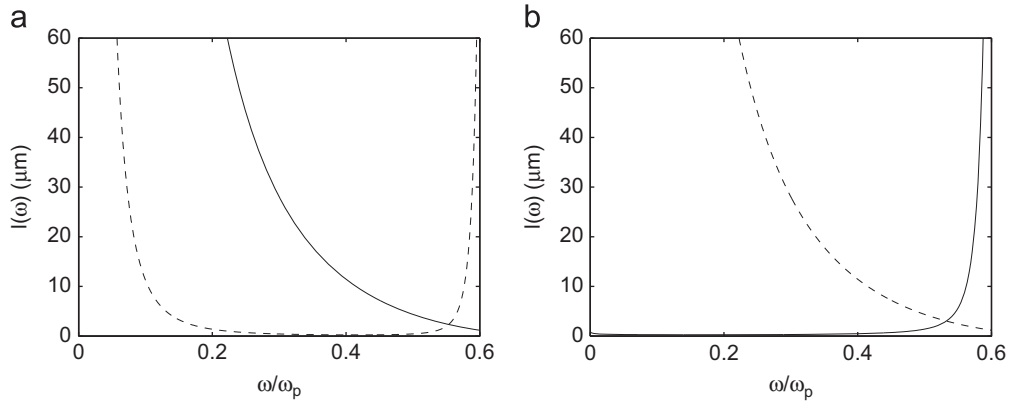

Fig. 3. Plots of the surface plasmon polariton propagation lengths due to radiative losses, $\ell_c(\omega)$ (——), and to ohmic losses, $\ell_p(\omega)$ (- - - - -), as functions of the dimensionless frequency ω/ω_p (a) $\ell_c(\omega)$ calculated on the basis of Eq. (11b); (b) $\ell_c(\omega)$ calculated on the basis of a numerical solution of Eq. (10). $R=0.5$ μm, $\omega_p=13.12\times10^{15}$ s^{-1}.

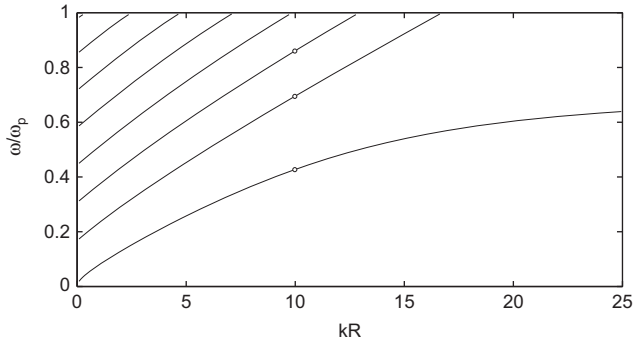

Fig. 4. The dispersion curves of the p-polarized surface plasmon polaritons propagating circumferentially on a portion of a cylindrical silver surface that is concave to the vacuum. $R=0.5$ μm, $\omega_p=13.12\times10^{15}$ s^{-1}.

of $(\omega/c)R$. For r in the region $r\geq R$ we seek a solution that decays to zero exponentially as r tends to infinity. It is necessary, therefore, to work in a frequency region in which $\varepsilon(\omega)$ is negative. The solution of Eq. (16b) in this frequency range that we choose is $K_\nu(|\varepsilon(\omega)|^{1/2}(\omega/c)r)$, where $K_\nu(x)$ is the modified Bessel function of the second kind and of order ν. The magnetic field in our system can then be written as

$$H_z(r,\theta|\omega)=AJ_\nu((\omega/c)r)\exp(i\nu\theta),\quad 0\leq r\leq R \tag{17a}$$

$$=BK_\nu(|\varepsilon(\omega)|^{1/2}(\omega/c)r)\exp(i\nu\theta),\quad r\geq R. \tag{17b}$$

Substitution of these expressions into the boundary conditions (4) yields the dispersion relation for p-polarized surface plasmon polaritons in this case in the form

$$\frac{K_\nu'(|\varepsilon(\omega)|^{1/2}(\omega/c)R)}{K_\nu(|\varepsilon(\omega)|^{1/2}(\omega/c)R)}=-|\varepsilon(\omega)|^{1/2}\frac{J_\nu'((\omega/c)R)}{J_\nu((\omega/c)R)}. \tag{18}$$

For real values of the order and arguments Eq. (18) is a real equation with real solutions. To solve it we rewrite it in the form $D_\nu(\omega)=0$, where

$$D_\nu(\omega)=1+|\varepsilon(\omega)|^{1/2}\frac{K_\nu(|\varepsilon(\omega)|^{1/2}(\omega/c)R)J_\nu'(\nu\omega/c)R)}{K_\nu'(|\varepsilon(\omega)|^{1/2}(\omega/c)R)J_\nu((\omega/c)R)}. \tag{19}$$

For a fixed real positive value of ν, $D_\nu(\omega)$ is calculated for values of ω increasing in a stepwise fashion in the interval $0\leq\omega\leq\omega_p$, and changes in its sign are sought. The values of ω at which this occurs are labeled by the index s in the order of their increasing magnitude. These calculations are repeated for a series of values of ν, and on the basis of their results the dispersion curves $\omega_s(\nu=kR)$ are constructed.

In Fig. 4 the results of such calculations are presented for the same values of the parameters R and ω_p that were used in obtaining Figs. 1–3. It is seen from these results that the dispersion curve consists of many branches. We can label these branches in the order of increasing frequency, as the 0, 1, 2, …, branches, with the lowest frequency branch labeled the 0 branch. The lowest frequency branch is the one that goes into the dispersion curve of the surface plasmon polariton at a planar vacuum–metal interface in the limit as $R\to\infty$.

As the radius R is increased the separation in frequency between consecutive branches of the dispersion curve decreases. Thus more branches crowd into the frequency range $0<\omega<\omega_p$.

The magnetic field $H_z(r,\theta|\omega)$ can now be written as

$$H_z(r,\theta|\omega)=Ae^{i\nu\theta}J_\nu((\omega/c)r),\quad 0\leq r\leq R \tag{20a}$$

$$=Ae^{i\nu\theta}\frac{J_\nu((\omega/c)R)}{K_\nu(|\varepsilon(\omega)|^{1/2}(\omega/c)R)}K_\nu(|\varepsilon(\omega)|^{1/2}(\omega/c)r),\quad r\geq R. \tag{20b}$$

The radial dependence of this field

$$R_p(r)=J_\nu((\omega/c)r),\ 0\leq r\leq R \tag{21a}$$

$$=\frac{J_\nu((\omega/c)R)}{K_\nu(|\varepsilon(\omega)|^{1/2}(\omega/c)R)}K_\nu(|\varepsilon(\omega)|^{1/2}(\omega/c)r),\quad r\geq R \tag{21b}$$

corresponding to the points $(kR=10,\omega/\omega_p=0.4274, kR=10,$ $\omega/\omega_p=0.6955$, and $kR=10,\omega/\omega_p=0.8611)$ marked by open circles on the three lowest frequency branches of the dispersion curve plotted in Fig. 4 is plotted as a function of r/R in Fig. 5. It is seen that these fields are localized to the surface in the sense that they decrease to zero exponentially with increasing distance into each medium from the interface. However, they have an oscillatory dependence on r/R in the immediate vicinity of the interface. In this region the field has nodes whose number equals the branch number. Thus the set of modes resembles the waveguide modes supported by a planar waveguide, with the mode that becomes the surface plasmon polariton in the limit $R\to\infty$ playing the role of the fundamental mode.

To explore how the preceding results are affected when the dielectric function of the metal is complex, $\varepsilon(\omega)=\varepsilon_1(\omega)+i\varepsilon_2(\omega)$, we replace Eq. (1) by the expression

$$\varepsilon(\omega)=1-\frac{\omega_p^2}{\omega(\omega+i\gamma)}, \tag{22}$$

so that

$$\varepsilon_1(\omega)=1-\frac{\omega_p^2}{\omega^2+\gamma^2} \tag{23a}$$

$$\varepsilon_2(\omega)=\frac{\gamma}{\omega}\frac{\omega_p^2}{\omega^2+\gamma^2}. \tag{23b}$$

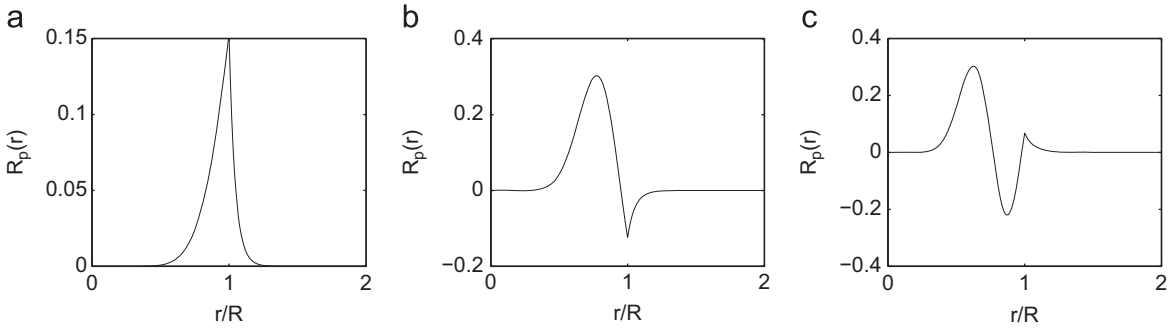

Fig. 5. The radial dependencies of the magnetic field $H_z(r,\theta|\omega)$ are plotted as functions of r/R for the values of ω/ω_p and kR indicated by the open circles on the three lowest frequency branches of the dispersion curve presented in Fig. 4.

By fitting Eqs. (23a) and (23b) to the values of $\varepsilon_1(\omega)$ and $\varepsilon_2(\omega)$ for silver at a wavelength $\lambda = 612.7$ nm, namely $\varepsilon_1(\omega) = -17.2$ and $\varepsilon_2(\omega) = 0.498$, we find that $\omega_p = 13.12 \times 10^{15}\ \mathrm{s}^{-1}$ and $\gamma = 0.8412 \times 10^{14}\ \mathrm{s}^{-1}$.

In solving the dispersion relation (18) the function $|\varepsilon(\omega)|$ must now be understood to be given by

$$|\varepsilon(\omega)| = -\varepsilon(\omega) = \left(\frac{\omega_p^2}{\omega^2+\gamma^2} - 1\right) - i\frac{\gamma}{\omega}\frac{\omega_p^2}{\omega^2+\gamma^2}. \tag{24}$$

It is convenient to write $|\varepsilon(\omega)|^{1/2}$ in the form

$$|\varepsilon(\omega)|^{1/2} = a_1(\omega) - ia_2(\omega), \tag{25}$$

where $a_1(\omega)$ and $a_2(\omega)$ are positive functions of ω.

In the visible region, e.g. at $\lambda = 612.7$ nm, $a_2(\omega)/a_1(\omega) \cong 1/60$.

Thus, to solve Eq. (18), we substitute Eq. (25) into Eq. (19), and use the approximations

$$K_\nu((\omega/c)R(a_1 - ia_2)) \cong K_\nu((\omega/c)Ra_1) - i(\omega/c)Ra_2K'_\nu((\omega/c)Ra_1)$$

$$K'_\nu((\omega/c)R(a_1 - ia_2)) \cong K'_\nu((\omega/c)Ra_1) - i(\omega/c)Ra_2K''_\nu((\omega/c)Ra_1),$$

to separate $D_\nu(\omega)$ into its real and imaginary parts, assuming ν to be real. The function $|D_\nu(\omega)|^{-2}$ is then plotted as a function of real $\nu$for a fixed value of ω. Peaks of this function occur at the values (s) of $\nu_R(\omega)$ corresponding to that value of ω. The width of each peak at half maximum is the corresponding value $2\nu_I(\omega)$. By varying ω in a systematic fashion curves of $\nu_R(\omega)$ and $\nu_I(\omega)$ were obtained.

In Fig. 6(a) we present results for ω/ω_p as a function of k_R for the branches of the dispersion curve plotted in Fig. 4. The solid curves are the results obtained with the use of a complex dielectric function, the dashed curves are the results obtained for a real dielectric function. These sets of curves are virtually indistinguishable on the scale of the figure. The use of a real dielectric function in these calculations is justified.

In Fig. 6(b) we present plots of the propagation distance of the surface wave corresponding to the lowest frequency branch of the dispersion curve in Fig. 4. The solid curve is the result obtained with a complex $\varepsilon(\omega)$. It reflects the attenuation of this wave in the presence of both radiative and ohmic losses. The dashed curve is the result obtained for the wave on the planar surface of a lossy metal surface. It reflects the attenuation of this wave due only to ohmic losses. It is seen that the radiative losses introduced by the curvature of the surface reduce the propagation distance resulting from ohmic losses alone. These results indicate that in calculations of the damping of a surface electromagnetic wave on a cylindrical surface it is important to include the imaginary part of the metal's dielectric function, especially in the low frequency limit.

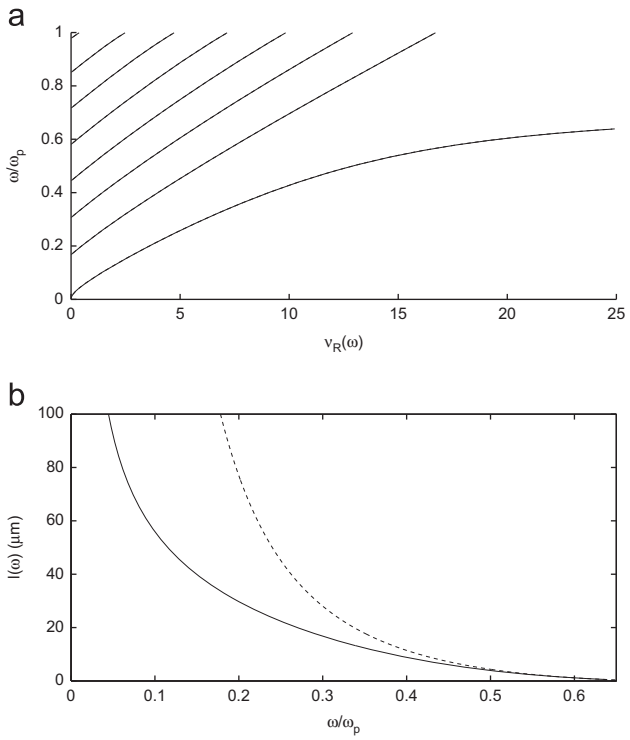

Fig. 6. (a) The dispersion curves of p-polarized surface plasmon polaritons propagating circumferentially on a portion of a cylindrical silver surface that is concave to the vacuum, calculated with a complex dielectric function defined by $\omega_p = 13.12 \times 10^{15}\ \mathrm{s}^{-1}$, $\gamma = 0.4812 \times 10^{14}\ \mathrm{s}^{-1}$, $R = 0.5$ μm (——); calculated with a real dielectric function defined by $\omega_p = 13.12 \times 10^{15}\ \mathrm{s}^{-1}$, $R = 0.5$ μm (- - - - -). (b) The propagation distance of the surface plasmon polariton corresponding to the lowest frequency branch of the dispersion curve depicted in (a), calculated with the same complex dielectric function on a silver surface concave to the vacuum (——), $R = 0.5$ μm, and on a planar lossy silver surface (- - - - -).

3. Discussion and conclusions

In this paper we have shown that the p-polarized surface-localized electromagnetic waves propagating circumferentially around a portion of a circularly cylindrical metal surface in contact with a vacuum that is either convex toward the vacuum or concave toward the vacuum have a complex structure. In the former case it consists of a leaky wave that is bound to the interface in the metal but radiates into the vacuum. In the latter case it consists of a discrete sequence of waves that are bound to the interface in both the metal and the vacuum, but have an oscillatory or standing wave form in the vicinity of the interface similar to the structure of the waves in a planar dielectric waveguide.

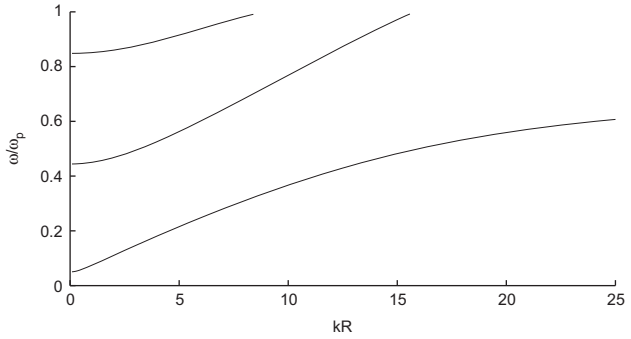

Fig. 7. The dispersion curves of the p-polarized surface plasmon polaritons propagating circumferentially on a portion of a cylindrical silver surface that is concave toward the vacuum given by the solution of Eq. (31). $R=0.5\,\mu$m, $\omega_p=13.12\times10^{15}\ s^{-1}$.

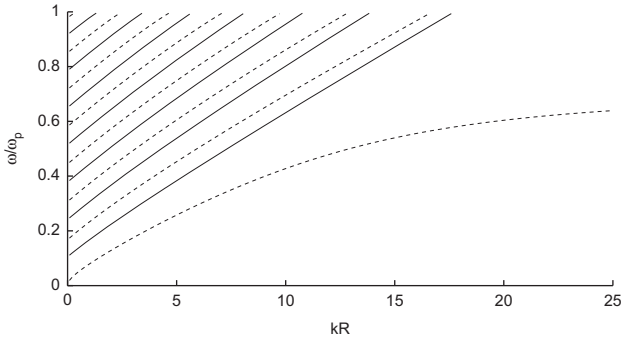

Fig. 8. The dispersion curves of the s-polarized waveguide plasmon polaritons studied in Ref. [7] (solid curves) and of the p-polarized waveguide plasmon polaritons plotted in Fig. 4 of the present paper (dashed curves). $R=0.5\,\mu$m, $\omega_p=13.12\times10^{15}\ s^{-1}$.

An understanding of the origin of the latter waves can be gained in the following way. We carry out the coordinate transformation $z=R\ln(r/R)$, and define $R^{\gtrless}(r)=f^{\gtrless}(z)=f^{\gtrless}(R\ln(r/R))$. The region $z>0$ corresponds to the region $r>R$, i.e. to the region of the metal, while the region $z<0$ corresponds to the region $0<r<R$, i.e. to the vacuum region. Eqs. (16) are then transformed into

$$\left[\frac{d^2}{dz^2}-k^2+\frac{\omega^2}{c^2}n_>(z)^2\right]f^>(z)=0,\quad z\geq0 \tag{26a}$$

$$\left[\frac{d^2}{dz^2}-k^2+\frac{\omega^2}{c^2}n_<(z)^2\right]f^<(z)=0,\quad z\leq0, \tag{26b}$$

where $k=\nu/R$, and

$$n_>(z)^2=\varepsilon(\omega)\exp(2z/R) \tag{27a}$$

$$n_<(z)^2=\exp(2z/R) \tag{27b}$$

are z-dependent refractive indices in the regions $z>0$ and $z<0$, respectively.

The boundary conditions satisfied by $f^{\gtrless}(z)$ become

$$f^>(z)|_{z=0}=f^<(z)|_{z=0} \tag{28a}$$

$$\frac{1}{\varepsilon(\omega)}\frac{df^>(z)}{dz}\bigg|_{z=0}=\frac{df^<(z)}{dz}\bigg|_{z=0}. \tag{28b}$$

In the immediate vicinity of the interface, where $|z|/R$ is small, Eqs. (26) take the forms

$$\left[\frac{d^2}{dz^2}-k^2+\varepsilon(\omega)\frac{\omega^2}{c^2}+2\varepsilon(\omega)\frac{\omega^2}{c^2}\frac{z}{R}\right]f^>(z)=0,\quad z>0 \tag{29a}$$

$$\left[\frac{d^2}{dz^2}-k^2+\frac{\omega^2}{c^2}+2\frac{\omega^2}{c^2}\frac{z}{R}\right]f^<(z)=0,\quad z<0. \tag{29b}$$

If we recall that $\varepsilon(\omega)$ is negative, the solutions of these equations are

$$f^>(z)=AAi\left(\left(\frac{Rc^2}{2|\varepsilon(\omega)|\omega^2}\right)^{2/3}\times\left(k^2+|\varepsilon(\omega)|\frac{\omega^2}{c^2}+2|\varepsilon(\omega)|\frac{\omega^2z}{c^2R}\right)\right),\quad z>0 \tag{30a}$$

$$f^<(z)=BAi\left(\left(\frac{Rc^2}{2\omega^2}\right)^{2/3}\left(k^2-\frac{\omega^2}{c^2}-2\frac{\omega^2}{c^2}\frac{z}{R}\right)\right),\quad z<0, \tag{30b}$$

where $Ai(z)$ is an Airy function. It is an exponentially decreasing function of z for $z>0$, and an oscillatory function of z for $z<0$. Thus we see from Eqs. (30) that for sufficiently large $|z|$ both $f^>(z)$ and $f^<(z)$ decrease exponentially with increasing distance from the interface $z=0$. The dispersion relation obtained from the boundary conditions (28) is

$$\frac{Ai\left(\left(\frac{Rc^2}{2\omega^2}\right)^{2/3}\left(k^2-\frac{\omega^2}{c^2}\right)\right)}{Ai'\left(\left(\frac{Rc^2}{2\omega^2}\right)^{2/3}\left(k^2-\frac{\omega^2}{c^2}\right)\right)}=|\varepsilon(\omega)|^{2/3}\frac{Ai\left(\left(\frac{Rc^2}{2|\varepsilon(\omega)|\omega^2}\right)^{2/3}\left(k^2+|\varepsilon(\omega)|\frac{\omega^2}{c^2}\right)\right)}{Ai'\left(\left(\frac{Rc^2}{2|\varepsilon(\omega)|\omega^2}\right)^{2/3}\left(k^2+|\varepsilon(\omega)|\frac{\omega^2}{c^2}\right)\right)}, \tag{31}$$

where the prime denotes differentiation with respect to argument. Eq. (31) has been solved numerically, and the resulting dispersion curve is plotted in Fig. 7 for the same values of the parameters used in obtaining Fig. 4. It is seen to consist of a multiplicity of branches like the dispersion curve plotted in Fig. 4. The quantitative differences between the two dispersion curves appear to be due to the approximations made in obtaining Eqs. (30).

Nevertheless this simple calculation suffices to show that a cylindrical vacuum–metal interface, with the metal concave to the vacuum, is equivalent to a planar interface between two graded index media that form a "potential well" in its vicinity that can bind one or more modes to it, depending on the frequency.

It has been shown in an earlier work [7] that a cylindrical vacuum–metal interface supports a series of guided wave-like modes of s polarization when the metal is concave toward the vacuum. In Fig. 8 we plot the dispersion curves of the s-polarized waveguide plasmon polaritons studied in Ref. [7] (solid curves) together with the dispersion curves of the p-polarized waveguide plasmon polaritons presented in Fig. 4 of the present paper (dashed curves). Both sets of curves have been calculated for the same values of ω_p and R. It is seen that for a given value of the surface wavenumber k the modes of the two polarizations occur in non-overlapping frequency regions. In fact, their dispersion curves interleave each other. Therefore, one and the same surface of this kind supports guided waves of both p and s polarizations, something that a planar vacuum–metal interface cannot do.

Acknowledgments

The research of J.P. and R.M.F. was supported in part by NOAA Educational Partnership Program for Minority Serving Institutions (EPP/MSI) Cooperative Agreement NAITAE 1623. The research of A. A.M. was supported in part by AFRL contract FA9453-08-C-0230.

Appendix A

In this Appendix we obtain an approximate analytic solution of Eq. (10) by an approach that differs from the one used by Berry for this purpose in Ref. [1], but which was suggested by him in that reference.

It is expected that if the surface is gently curved $k_R(\omega)/R$ will be very close to the value $k_R(\omega)=(\omega/c)[|\varepsilon(\omega)|/(|\varepsilon(\omega)|-1)]^{1/2}$ it has for a planar surface. We will see below that this is indeed the case. This means that $k_R(\omega)>(\omega/c)$. For a gently curved surface both the order $k_R(\omega)R$ and the argument $(\omega/c)R$ of the Hankel functions in Eq. (10) are large, but since $k_R(\omega)>(\omega/c)$ we have the case of "argument smaller than order, order large". Thus we have to use expressions for the Hankel functions appropriate to this situation. Since $H_\nu^{(1)}(z)=J_\nu(z)+iY_\nu(z)$, these expressions are given by the Debye formulas given by Eqs. (9.3.7) and (9.3.11) of Abramowitz and Stegun [6],

$$J_\nu(\nu\ \mathrm{sech}\ \alpha)\sim\frac{e^{-\nu(\alpha-\tanh\alpha)}}{\sqrt{2\pi\nu\tanh\alpha}} \tag{A.1a}$$

$$J_\nu'(\nu\ \mathrm{sech}\ \alpha)=\frac{\sqrt{\sinh\alpha\cosh\alpha}}{\sqrt{2\pi\nu}}e^{-\nu(\alpha-\tanh\alpha)}, \tag{A.1b}$$

respectively, and by Eqs. (9.3.8) and (9.3.12) of Ref. [6]

$$Y_\nu(\nu\ \mathrm{sech}\ \alpha)\sim-\frac{2e^{\nu(\alpha-\tanh\alpha)}}{\sqrt{2\pi\nu\tanh\alpha}} \tag{A.2a}$$

$$Y_\nu'(\nu\ \mathrm{sech}\ \alpha)\sim\frac{2\sqrt{\sinh\alpha\cosh\alpha}}{\sqrt{2\pi\nu}}e^{\nu(\alpha-\tanh\alpha)}, \tag{A.2b}$$

respectively, where

$$\mathrm{sech}\ \alpha=\frac{\omega R}{c\nu}. \tag{A.3}$$

It follows that

$$\sinh\alpha=[(c\nu/\omega R)^2-1]^{1/2} \tag{A.4a}$$

$$\cosh\alpha=(c\nu/\omega R) \tag{A.4b}$$

$$\tanh\alpha=\frac{[(c\nu/\omega R)^2-1]^{1/2}}{(c\nu/\omega R)} \tag{A.4c}$$

$$\alpha=\frac{1}{2}\ln\frac{(c\nu/\omega R)+\sqrt{(c\nu/\omega R)^2-1}}{(c\nu/\omega R)-\sqrt{(c\nu/\omega R)^2-1}}. \tag{A.4d}$$

We also assume that ν is in the region $\nu>|\varepsilon(\omega)|^{1/2}(\omega R/c)$. The asymptotic formulas for $I_\nu(z)$ and $I_\nu'(z)$ for the case $\nu>z$ are given by Eqs. (9.7.7) and (9.7.9) of Abramowitz and Stegun [6],

$$I_\nu(\nu\beta)\sim\frac{1}{\sqrt{2\pi\nu}}\frac{e^{\nu\eta}}{(1+\beta^2)^{1/4}} \tag{A.5a}$$

$$I_\nu'(\nu\beta)\sim\frac{1}{\sqrt{2\pi\nu}}\frac{(1+\beta^2)^{1/4}e^{\nu\eta}}{\beta}, \tag{A.5b}$$

respectively, where

$$\beta=|\varepsilon(\omega)|^{1/2}(\omega R/c\nu) \tag{A.6}$$

and

$$\eta=\sqrt{1+\beta^2}+\ln\frac{\beta}{1+\sqrt{1+\beta^2}}. \tag{A.7}$$

With the use of these results we now rewrite Eq. (10) in the form

$$\frac{(1+\beta^2)^{1/2}}{\beta}=|\varepsilon(\omega)|^{1/2}\sinh\alpha\frac{1-\frac{i}{2}e^{-2\nu(\alpha-\tanh\alpha)}}{1+\frac{i}{2}e^{-2\nu(\alpha-\tanh\alpha)}}. \tag{A.8}$$

If we neglect the exponentially small terms on the right-hand side of this equation, which is equivalent to approximating $H_\nu^{(1)}(z)$ by $iY,(z)$, Eq. (A.8) becomes

$$[|\varepsilon(\omega)|+(c\nu/\omega R)^2]^{1/2}=|\varepsilon(\omega)|[(c\nu/\omega R)^2-1]^{1/2}, \tag{A.9}$$

whose solution is

$$\frac{\nu_R(\omega)}{R}=\frac{\omega}{c}\left[\frac{|\varepsilon(\omega)|}{|\varepsilon(\omega)|-1}\right]^{1/2}, \tag{A.10}$$

without any imaginary part $\nu_I(\omega)/R$. This is why we have denoted this solution as $\nu_R(\omega)/R$.

We now return to Eq. (A.8), which we rewrite as

$$\frac{[|\varepsilon(\omega)|+(c\nu/\omega R)^2]^{1/2}}{|\varepsilon(\omega)|[(c\nu/\omega R)^2-1]^{1/2}}=\frac{1-ix}{1+ix} \tag{A.11}$$

where, to simplify the notation, we have introduced the variable x defined by

$$x=\tfrac{1}{2}\exp[-2\nu(\alpha-\tanh\alpha)]. \tag{A.12}$$

On the left-hand side of Eq. (A.11) we replace ν by $\nu_R+i\nu_I$. With this substitution Eq. (A.11) becomes

$$\frac{[|\varepsilon(\omega)|+(c\nu_R/\omega R)^2]^{1/2}}{|\varepsilon(\omega)|[(c\nu_R/\omega R)^2-1]^{1/2}}\frac{\left[1+2i\dfrac{(c\nu_R/\omega R)^2}{|\varepsilon(\omega)|+(c\nu_R/\omega R)^2}\dfrac{\nu_I}{\nu_R}\right]^{1/2}}{\left[1+2i\dfrac{(c\nu_R/\omega R)^2}{(c\nu_R/\omega R)^2-1}\dfrac{\nu_I}{\nu_R}\right]^{1/2}}=\frac{1-ix}{1+ix}. \tag{A.13}$$

The first factor on the left-hand side of this equation is equal to unity in view of Eq. (A.10). The equation for ν_I/ν_R then becomes

$$\left[\frac{(c\nu_R/\omega R)^2}{(c\nu_R/\omega R)^2-1}-\frac{(c\nu_R/\omega R)^2}{(c\nu_R/\omega R)^2+|\varepsilon(\omega)|}\right]\frac{\nu_I}{\nu_R}=2x, \tag{A.14}$$

which with the use of Eqs. (A.4c), (A.4d) and (A.10) becomes

$$\frac{\nu_I(\omega)}{R}=\frac{\nu_R(\omega)}{R}\frac{|\varepsilon(\omega)|}{(|\varepsilon(\omega)|-1)(|\varepsilon(\omega)|+1)}\times\exp\left\{-2R\frac{\nu_R(\omega)}{R}[\alpha-\tanh\alpha]\right\} \tag{A.15a}$$

$$=\frac{\omega}{c}\frac{|\varepsilon(\omega)|^{3/2}}{(|\varepsilon(\omega)|-1)^{3/2}(|\varepsilon(\omega)|+1)}\times\exp\left\{-\frac{(\omega/c)R}{(|\varepsilon(\omega)|-1)^{1/2}}\left[|\varepsilon(\omega)|^{1/2}\ln\frac{|\varepsilon(\omega)|^{1/2}+1}{|\varepsilon(\omega)|^{1/2}-1}-2\right]\right\}. \tag{A.15b}$$

This is the result obtained by Berry by the use of a physically based approach. Berry has shown that the use of the Debye approximation for $H_{\nu_R}((\omega/c)R)$, which requires that $\nu_R>(\omega/c)R$, is valid for the case where $\varepsilon(\omega)$ has the simple free electron form, Eq. (1), provided that $|\varepsilon(\omega)|\ll(\omega R/2c)^{2/3}$,which is equivalent to $\omega>\omega_p(2c/\omega R)^{1/3}$.

References

[1] M.V. Berry, J. Phys. A: Math. Gen. 8 (1975) 1952.
[2] P.B. Johnson, R.W. Christy, Phys. Rev. B 6 (1972) 4370.
[3] G. Arfken, Mathematical Methods for Physicists, 3rd ed., Academic Press, New York, 1985, p. 310, 963–964.
[4] A. Cuyt, V.B. Petersen, B. Verdonk, H. Waadeland, W.B. Jones, Handbook of Continued Fractions for Special Functions, Springer-Verlag, New York, 2008.
[5] A. Gil, J. Segura, N.M. Temme, Numerical Methods for Special Functions, SIAM, Philadelphia, PA, 2007.
[6] M. Abramowitz, I.A. Stegun (Eds.), Handbook of Mathematical Functions, Dover, New York, 1964.
[7] J. Polanco, R.M. Fitzgerald, A.A. Maradudin, Phys. Lett. A 376 (2012) 1573.